

IPO-LDM: Depth-aided 360-degree Indoor RGB Panorama Outpainting via Latent Diffusion Model

Tianhao Wu*, Chuanxia Zheng[†], and Tat-Jen Cham*
 *Nanyang Technological University, [†]University of Oxford



Figure 1. **Example results of our IPO-LDM on various masks** (masked regions shown in blue that is transparent for better visualization). Our IPO-LDM model not only effectively generates semantically meaningful content and plausible appearances with many objects, such as beds, sofas and TV’s, but also provides multiple and diverse solutions for this ill-posed problem. (Zoom in to see the details.)

Abstract

Generating complete 360° panoramas from narrow field of view images is ongoing research as omnidirectional RGB data is not readily available. Existing GAN-based approaches face some barriers to achieving higher quality output, and have poor generalization performance over different mask types. In this paper, we present our 360° indoor RGB panorama outpainting model using latent diffusion models (LDM), called IPO-LDM. We introduce a new bi-modal latent diffusion structure that utilizes both RGB and depth panoramic data during training, but works surprisingly well to outpaint normal depth-free RGB images during inference. We further propose a novel technique of introducing progressive camera rotations during each diffusion denoising step, which leads to substantial improvement in achieving panorama wraparound consistency. Results show that our IPO-LDM not only significantly outperforms state-of-the-art methods on RGB panorama outpainting, but can also produce multiple and diverse well-structured results for different types of masks. The code will be released soon. And our project page is at <https://sm0kywu.github.io/ipoldm/>.

1. Introduction

Omnidirectional 360° RGB panoramas are helpful for various applications, such as lighting estimation [9, 8, 32] and new scene synthesis [31] in AR and VR. An obvious limitation, however, is that capturing, collecting and restoring such extensive datasets with 360° images is a high-effort and high-cost undertaking [1, 2], while manually creating a 3D space from scratch can be a demanding task [18, 4, 24].

To reduce the cost of collecting large 360° datasets, the latest learning methods [1, 31, 2, 25] have been proposed, focusing on generating omnidirectional RGB panoramas from narrow field of view (NFOV) images. These methods are typically built upon Generative Adversarial Networks (GANs) [10], which have achieved remarkable success in creating new content. However, GAN architectures face some notable problems, including 1) mode collapse (seen in Fig. 1(c)), 2) unstable training [30], and 3) difficulty in generating multiple structurally reasonable objects [6], which hinder its performance on synthesizing complex scenes (Fig. 1).

In this paper, we propose an alternative method for 360° indoor RGB panorama outpainting via the latest latent diffusion models (LDMs) [29], called IPO-LDM. An important insight here is that a diffusion model directly adds noise

to the spatial images or features through a Markov Chain over T steps, which results in a *stable training of a generative model with consistent spatial resolution in each step*. This characteristic is critical in our 360° panorama scenario, as it preserves the spatial information necessary for generating structurally reasonable objects. Although recent works have already applied diffusion models in image inpainting tasks [21, 19], it remains a challenge to directly apply them in our setting.

Unlike previous inpainting works [26, 35, 21], generating a 360° panorama from an NFoV image faces greater challenges: 1) the outpainting mask is *significantly larger* than traditional inpainting and 2) *semantically reasonable objects have to be generated* within the scene, instead of filling in with generic background textures which will create empty rooms (as shown in Fig. 1 (c)). To achieve this, we creatively introduce depth information when *training* the diffusion model to aid the RGB generation. Our *key motivation* for doing so is that the depth information is crucial for helping the network understand the physical structure of objects and the layout of the scene [28].

Conversely, our proposed IPO-LDM *does not* depend on depth input at all during *inference* (Fig. 2(b)), which enables applications such as panoramic outpainting from normal photos taken by casual users. Despite this lack of depth input, when compared to the state-of-the-art BIPS [25], which uses depth for both training and testing, our method was able to achieve significant improvement on RGB outpainting (as seen in Fig. 1). While we recognize BIPS as being more focused on outpainting RGB-D panoramas, it is nonetheless rather interesting that even in the extreme case when the full ground-truth depth is provided to BIPS, and no depth is provided to our method, it is still able to achieve generally better RGB outpainting performance (Table 2b).

Another challenge of this task is the unique characteristic of panorama images: 3) the two ends of the image must be aligned to ensure the integrity and *wraparound consistency* of the entire space, *i.e.* the indoor scene itself does not have a beginning and an end. We present two strategies to enhance this property in the generated results. During the training process, a *camera-rotation* approach is used to randomly crop and stitch the images for data augmentation (Fig. 4). It encourages the networks to capture information from different views in a 360° panorama. More importantly, a *two-end alignment* mechanism is applied at each step of the denoising process (Fig. 5), which explicitly enforces the two ends of an image to be wraparound-consistent.

We evaluate the proposed method on the Structured3D dataset [37]. Experimental results demonstrate that our IPO-LDM not only significantly outperforms previous state-of-the-art 360° RGB panorama outpainting or inpainting methods, but is also able to provide multiple and diverse well-structured results for different types of masks (Fig. 1).

In summary, our main contributions are as follows:

- A new bi-modal latent diffusion structure that utilizes both RGB and depth panoramic data to better learn spatial layouts and patterns during training, but works surprisingly well to outpaint normal depth-free RGB images during inference;
- A novel technique of introducing progressive camera rotations during *each* diffusion denoising step, which leads to substantial improvement in achieving panorama wraparound consistency;
- Our IPO-LDM not only significantly outperforms state-of-the-art methods on RGB panorama outpainting, but can also produce diverse well-structured results for different mask types.

2. Related Work

2.1. Image Inpainting/Outpainting

Early image inpainting approaches [5, 12] tended to focus on mining the input image for low-level patterns or clues to fill in missing areas. However, these methods often assume that the missing patches can be replicated from visible parts. These models usually do not work well in generating new content, nor capable of performing large-scale completion.

Since the introduction of GANs [10], most in/outpainting methods [16, 20, 26, 17] started adopting the encoder-decoder + adversarial training approach, resulting in substantial progress. More recently, the denoising diffusion probabilistic model (DDPM) is an emerging alternative for generative modeling [14], outperforming even GAN-based methods [3] for image synthesis. When applied to image outpainting, we can consider methods to fall into the two categories below:

Mask-conditional. Here the DDPM is trained to outpaint conditioned on the input mask. The image is typically masked before the denoising stage, with the DDPM then trained to generate results that are visually consistent with the original image. A disadvantage is that such approaches can be sensitive to the training mask distribution, responding poorly to out-of-distribution masks.

Unconditional. RePaint [21] used an unconditionally trained DDPM. Specifically, instead of learning a mask-conditional generative model, the generative process is conditioned by sampling from the given pixels during the reverse diffusion iterations. Therefore, the model is not trained for the inpainting task itself and can better handle out-of-distribution masks.

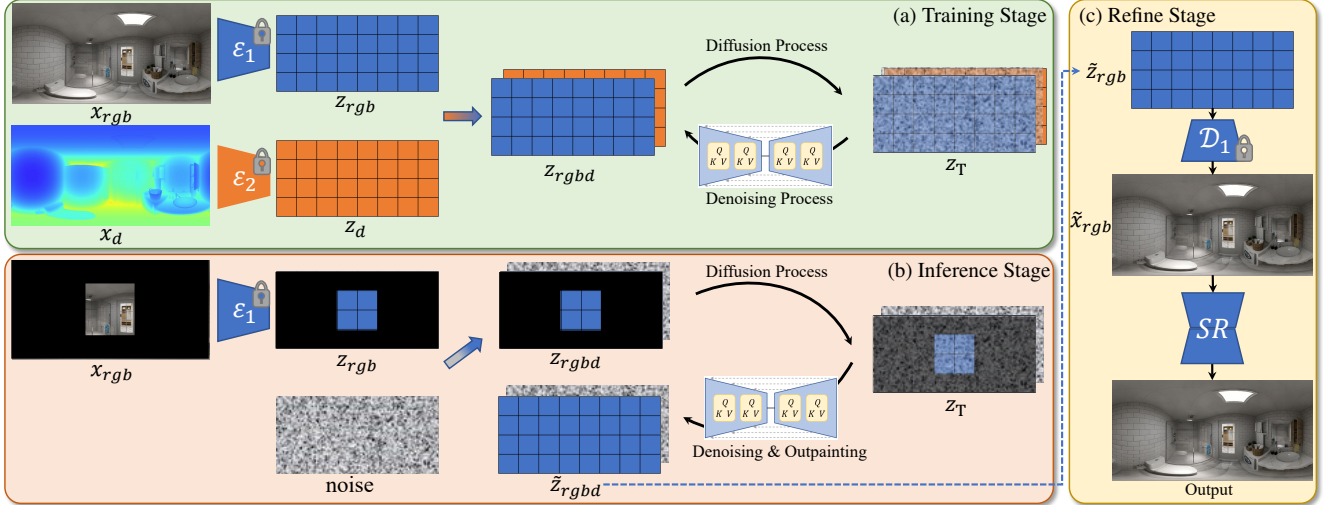


Figure 2. **The overall pipeline of our proposed IPO-LDM method.** (a) During training, no masks are used, and depth information is applied to aid in completing RGB panorama synthesis. (b) However, during inference, the depth information is no longer needed for masked RGB panorama outpainting. (c) Additionally, a super-resolution model is implemented to further enhance the high-resolution outpainting. Note that the VQ-based encoder-decoders are pre-trained in advance, and fixed in the rest of our framework (identified as “locked”).

2.2. 360° Panorama Image Outpainting

Unlike normal images, 360° images are subjected to equirectangular projection. As a result, all objects and layouts in the images are distorted to varying amounts depending on placement, more so nearer the top and bottom poles. The generated image has to not only maintain the distorted structure but also be visually plausible, with the two ends also needing to be wraparound-consistent. Some works [1, 31] are focused on deterministic completion of 360° RGB images, with BIPS [25] further extending this to RGB-D panorama synthesis. In order to generate diverse results, SIG-SS [11] uses a symmetry-informed CVAE, while OmniDreamer [2] uses transformer-based sampling. Both require additional mechanisms to achieve this goal. For DDPM, every reverse diffusion step is inherently stochastic since it incorporates noise from a Gaussian distribution, giving diverse results.

2.3. Latent Diffusion

LDMs [29] can be trained on larger image scales because they perceptually compress images into a smaller latent space with lower diffusion cost. Given an image in RGB space, the encoder \mathcal{E} maps x into a latent representation $z = \mathcal{E}(x) \in \mathbb{R}^{h \times w \times c}$. In contrast to previous works [7, 27] that relied on an arbitrary 1D ordering of the learned space z to model its distribution autoregressively, the inherent spatial structure of the image does not change but is downsampled during this process, with the decoder \mathcal{D} used for returning to higher resolutions. Two different kinds of regularization, KL-reg and VQ-reg, were experimented with in

[29]. In our work, we chose to use the VQ model, which uses a vector quantization layer [34] within the decoder. As stated in [29], it can be interpreted as a VQGAN [7] but with the quantization layer absorbed by the decoder.

3. Methods

Given a 360° image $x \in \mathbb{R}^{H \times W \times C}$, degraded by a number of missing pixels to become a masked image x_m , our main goal is to infer semantically meaningful content for the missing regions, while simultaneously generating visually realistic appearances. This task is conceptually similar to conventional learning-based image inpainting, but this setting faces greater challenges due to the following three differences: 1) our **output** is a 360° *panorama image with wraparound consistency*, rather than a typical NFoV image; 2) the outpainting **mask** is *significantly larger* than those used in traditional inpainting; 3) our **goal** is to *generate multiple appropriate objects* within a scene, instead of simply replacing objects with generic background.

To address these challenges, we propose a novel framework, called IPO-LDM. As depicted in Fig. 2(a), the training stage starts with two branches for RGB and depth. In each branch, the input is embedded into the latent space prior to the discrete layer in the corresponding pre-trained VQ model, following [29]. These representations are then combined to form $z_{rgb,d}$, which undergoes diffusion to obtain z_T . The resulting z_T is inversely denoised back to the original latent domain through a trained UNet+attention structure. Finally, the pre-trained decoder is employed to rebuild the full RGB-D results.

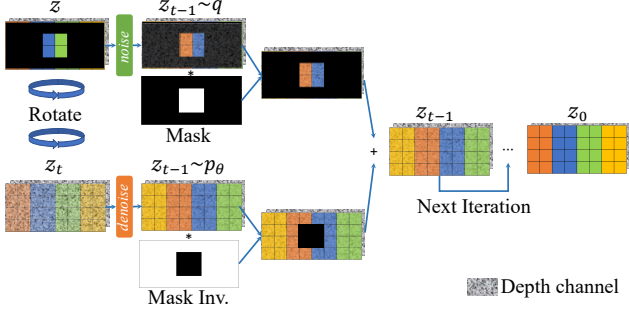


Figure 3. **LDM outpainting structure.** In each step, we sample the known region from the encoded latent input (above) and the unknown part from the DDPM output (below). The depth map is *not* necessary during the inference, which is set as random noise.

During inference, our system takes a masked RGB image, and conducts panoramic outpainting. Note that our proposed model does *not* require harder-to-acquire depth maps as input, needing only a noise map (Fig. 2(b)). The output is then super-resolved into the final image in a refinement stage (Fig. 2(c)).

3.1. Latent Diffusion Outpainting

As mentioned, current diffusion-based inpainting methods [21, 15] are often restricted to small image sizes, typically up to 256×256 . Additionally, these approaches do not ensure *wraparound consistency* during completion, which is crucial for 360° panoramas. Finally, they do *not* work well for producing multiple objects within large masks.

In order to perform our task on 512×1024 panoramas, we extend RePaint [21] to latent space outpainting. This is possible because the partially visible regions are not changed during perceptual image compression. Note that the 360° wraparound consistency is still preserved in both the pixel and latent domains, which is important for our setting. To further ensure such a wraparound consistency, a rotational outpainting mechanism is introduced in Sec. 3.2.

The diagram of our latent diffusion outpainting method is shown in Fig. 3. Let x denote the original visible image, while $m \odot x$ and $(1 - m) \odot x$ represent the missing and visible pixels, respectively. The latent input z is then defined as $z = \mathcal{E}_\theta((1 - m) \odot x)$. In the completion task, we expect the model to *generate plausibly reasonable content for the missing regions, while preserving the visible information as much as possible*. Therefore, we add a step-dependent amount of Gaussian noise to the known regions, while denoising the previous latent vector for one step. To combine them, the mask is first downscaled to the latent vector size m_d , with the noised and denoised results then processed by the mask and inverse mask respectively. For each outpainting step, the process can be described by the following expressions:

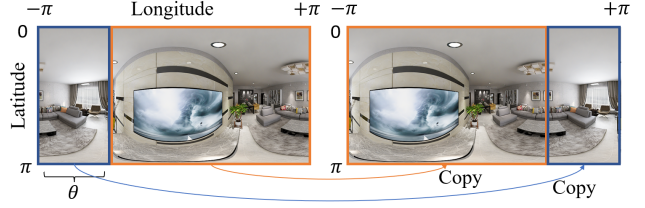


Figure 4. **Camera-rotation.** During training, we randomly crop θ degree from the left and stitch to the right for data augmentation.

$$z_{t-1}^{known} \sim q(z_t | z_{t-1}), \quad (1)$$

$$z_{t-1}^{unknown} \sim p_\theta(z_{t-1} | z_t), \quad (2)$$

$$z_{t-1} = m_d \odot z_{t-1}^{known} + (1 - m_d) \odot z_{t-1}^{unknown}. \quad (3)$$

Here, q is the forward distribution in the diffusion process and p_θ is the inverse distribution. After T iterations, z_0 is restored to image space using the pre-trained VQ decoder.

3.2. Camera-rotation and Two-end Alignment Mechanism for 360° Panorama

Since 360° panoramas are meant to be wraparound consistent, we apply a *circular shift* data augmentation, called camera-rotation, to the panorama image dataset (examples shown in Fig. 4), to enhance the model’s performance. In particular, we randomly select a rotation angle, and use it to crop and re-stitch the patch to produce a new panorama.

While camera-rotation may improve the model’s implicit understanding of the expected wraparound consistency by providing a large number of data-augmented examples, it still does not impose strong enough constraints on wraparound alignment of the results. Therefore, in the inference processing, we propose a *novel two-end alignment mechanism* that can be naturally combined with our latent diffusion outpainting process.

The denoising process of DDPM consists of a number of iterations, rather than a single step. During *each iteration*, we apply the camera-rotation operation to rotate both the latent vectors and masks by 90° , before performing an outpainting step. This procedure more effectively connects the two ends of the panorama from the previous step, which encourages the model to take into account the condition that the two ends are actually connected and generate aligned ends. Instead of changing the size of the images, generating overlapping content, or introducing extra loss functions, we provide ‘hints’ to the model by rotating the panorama horizontally, thus enhancing the effect of alignment at both ends (examples shown in Fig. 5).

3.3. Bi-modal Latent Diffusion Model

In order to introduce depth information to aid RGB generation, perhaps a simple idea would be to use depth infor-

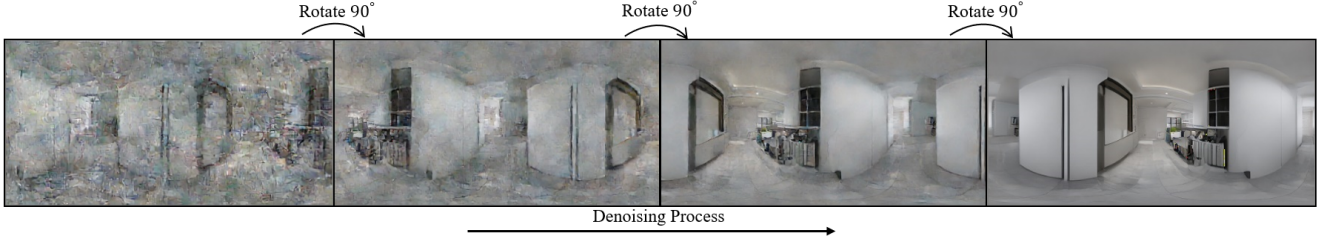


Figure 5. **An example of our two-end alignment mechanism.** During inference, we rotate the scene for 90° for *each* denoising step, so that the full denoising diffusion process will effectively achieve wraparound consistency.

mation as an explicit condition during training and inference. The depth information may be compressed into latent space and then introduced into the denoising process of the RGB images via cross-attention. However, through experiments, we have found that such an approach often leads to blurry results (Fig. 8). Meanwhile, using two parallel LDMs to reconstruct depth and RGB images separately, together with a joint loss, may also appear to be an intuitive solution. However, this idea is difficult to implement due to the computational resource requirements of multiple LDMs.

Therefore we designed a bi-modal latent diffusion structure to introduce depth information while generating high-quality RGB output, but which is *needed only during training*. Specifically, we trained two separate VQ models for RGB and depth images, and then concatenate $z_{rgb} \in \mathbb{R}^{h \times w \times 3}$ with $z_{depth} \in \mathbb{R}^{h \times w \times 1}$ at the latent level to get $z_{rgbld} \in \mathbb{R}^{h \times w \times 4}$. The training of VQ models are exactly the same as in LDM with downsampling factor $f=4$. Then we follow the standard process to train an unconditional DDPM with z_{rgbld} via a variant of the original LDM loss:

$$L_{RGB-D LDM} := \mathbb{E}_{z_{rgbld}, \epsilon \sim \mathcal{N}(0,1), t} [\|\epsilon - \epsilon_\theta(z_t, t)\|_2^2], \quad (4)$$

$$z_{rgbld} = \text{Cat}(\mathcal{E}_1(x_{rgb}); \mathcal{E}_2(x_{depth}))$$

Reconstructed RGB-D images can be obtained by decoupling z_{rgbld} and decoding. It is important to note that during training, we use the full RGB-D image as input, *without masks*. Conversely during the inference stage, the model can perform outpainting of the masked RGB image directly *without any depth input*, with the fourth channel of z_{rgbld} replaced by random noise.

3.4. RefineNet

Although mapping images to a smaller latent space via an autoencoder prior to diffusion can save training space and thus allow larger size inputs, the panorama size of 512×1024 is still a heavy burden for LDM [29]. Therefore, we adopt a two-stage approach to complete the outpainting task. Initially, the original input is downscaled to 256×512 as the input to the LDM. Correspondingly, the image size of the LDM output is also 256×512 . Therefore, an additional module is needed to upscale the output image size to



Figure 6. **Examples of various mask types.** See text for details.

512×1024 . Traditional interpolation methods often lead to blurry results. Also, since panorama images are distorted and the objects and layouts do not follow the regular image patterns, we trained a super-resolution GAN model specifically for panoramas, in order to produce visually plausible results at a higher resolution.

4. Experiments

4.1. Experimental Details

Dataset. We estimated our model on the Structured3D dataset [37], which provides 360° indoor RGB-D data with a 512×1024 resolution. We split the dataset into 16930 train, 2116 validation, and 2117 test instances.

Metrics. Due to large masks, we should not require the completed image to be exactly the same as the original image, since there are many plausible solutions (*e.g.* new furniture and ornaments, and their placement). Therefore, we mainly report the following dataset-level metrics: 1) Fréchet Inception Distance (FID) [13], 2) Spatial FID (sFID) [23], 3) density and coverage [22]. FID compares the distance between distributions of generated and original images in a deep feature domain, while sFID is a variant of FID that uses spatial features rather than the standard pooled features. Additionally, density reflects how accurate the generated data is to the real data stream, while coverage reflects how well the generated data generalizes the real data stream.

Mask Types. Most works focused on generating omnidirectional images from N FoV images (Fig. 6(a)). However, partial observability may also occur due to sensor damage in 360° cameras. Such masks can be roughly simulated by randomly sampling a number of N FoV camera views within

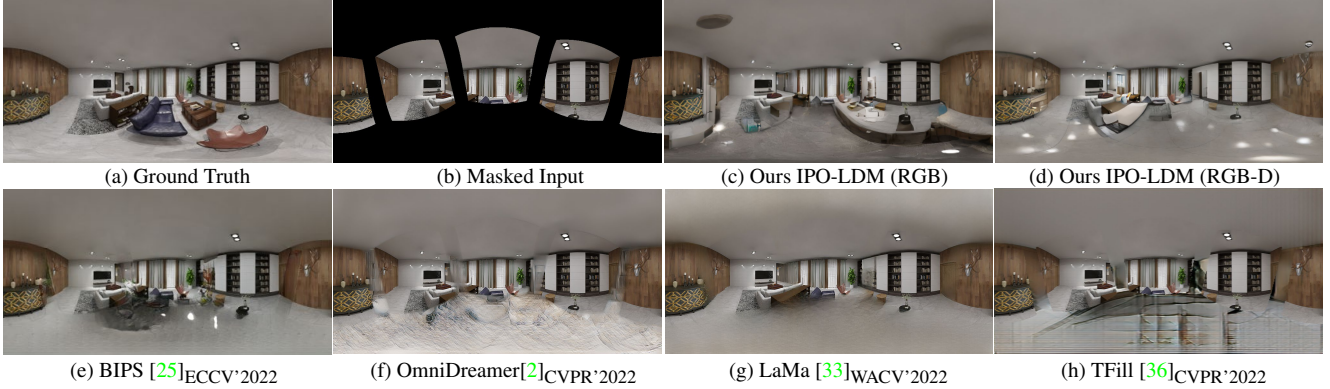


Figure 7. **Qualitative comparison for RGB panorama outpainting.** Our IPO-LDM generated more objects with appropriate layout, and with better visual quality. Please zoom in to see the details. More comparisons are provided in the supplementary material.

Methods	Training Data	FID ↓	sFID ↓	Density ↑	Coverage ↑
BIPS	RGB+D	68.79	42.62	0.306	0.412
OmniDreamer	RGB	65.47	37.04	0.14	0.175
LaMa	RGB	115.92	107.69	0.034	0.082
TFill	RGB	83.84	61.40	0.075	0.086
IPO-LDM (RGB)	RGB	24.33	29.00	0.667	0.635
IPO-LDM (RGB-D)	RGB+D	21.55	26.95	0.867	0.708

Table 1. **Quantitative results for RGB outpainting.** All models were tested without depth input.

the panorama (Fig. 6(b)). We also experimented with other types of masks, such as randomly generated regular masks (Fig. 6(c)). Finally, the regions with floors and ceilings in panoramic images are often less interesting than the central regions. Hence we also generated layout masks which muffle all areas except floors and ceilings, to more incisively test the model’s generative power (Fig. 6(d)).

Baseline Models. We mainly compared with the following state-of-the-art methods: including inpainting models LaMa [33]_{WACV’2022} and TFill [36]_{CVPR’2022}, panorama outpainting models BIPS [25]_{ECCV’2022} and OmniDreamer [2]_{CVPR’2022}. All models are retrained on the Structured3D dataset using their publicly available codes.

Implementation Details. To verify the auxiliary effect of depth training input on RGB image generation, we trained two different versions of IPO-LDM, 1) IPO-LDM (RGB) and 2) IPO-LDM (RGB-D). The RGB-D version follows Fig. 2, while the RGB version excludes depth altogether.

4.2. Main Results

Table 1 shows the quantitative comparison of RGB panorama outpainting on the Structured3D dataset with camera masks. For a fair comparison, all models are evaluated without depth maps during testing. As can be seen, the proposed IPO-LDM model significantly outperforms all



Figure 8. **Outpainting with a basic depth-conditioned LDM.** This leads to blurry results, see text for details.

state-of-the-art models. Specifically, the FID score is substantially better (relative 67.0% improvement).

The effectiveness is also clearly visualized in Fig. 7. For BIPS [25] and OmniDreamer [2], the generated areas hold obvious gaps to the original visible regions. As for LaMa [33] and TFill [36], they output blurry results for large invisible areas. Compared to them, our IPO-LDM produces more natural results in terms of transition, as well as more realistic floor texture and a more logical and clearer sofa in the central area. Comparing the RGB and RGB-D versions of our IPO-LDM, in Fig. 7(c), there are some step-like artifacts on the ground in the RGB version. In contrast, the same region of RGB-D result (Fig. 7(d)) appears more structurally appropriate. The transitions between the items, walls, ceiling, and floor are also more natural. Such improvement proves the advantages of jointly learning to synthesize depth data along with RGB images, *even when depth is not used during test time.*

4.3. Ablation Experiments

We ran a number of ablations to analyse the effectiveness of each core component in our IPO-LDM. Results are shown in Tables 2a, 2b, and 2c, and Figs. 8 and 9.

Depth Maps. We first evaluated the importance of depth maps in panoramic outpainting, reported in Table 2b. We also compared with the state-of-the-art BIPS [25], as it was also trained with RGB-D images. Besides, we have

Methods	Camera Mask				NFoV Mask				Layout Mask				Random Box Mask			
	FID ↓	sFID ↓	D ↑	C ↑	FID ↓	sFID ↓	D ↑	C ↑	FID ↓	sFID ↓	D ↑	C ↑	FID ↓	sFID ↓	D ↑	C ↑
BIPS (with depth)	31.70	28.89	0.769	0.660	57.69	44.68	0.205	0.277	32.25	24.66	0.645	0.579	25.35	22.60	0.676	0.798
BIPS (w/o depth)	68.79	42.62	0.306	0.412	98.48	51.15	0.075	0.109	34.91	25.83	0.596	0.561	43.17	24.25	0.613	0.771
OmniDreamer	65.47	37.04	0.143	0.175	62.56	36.24	0.125	0.184	82.71	28.40	0.103	0.120	45.10	24.12	0.329	0.576
LaMa	115.92	107.69	0.034	0.082	125.77	136.32	0.002	0.006	129.77	35.23	0.018	0.043	45.25	24.21	0.429	0.701
TFill	83.84	61.40	0.075	0.086	93.62	76.13	0.037	0.027	97.99	43.40	0.046	0.052	46.84	30.72	0.368	0.574
IPO-LDM (RGB)	24.33	29.00	0.667	0.635	24.01	30.00	0.639	0.617	25.37	22.92	0.785	0.677	17.88	21.21	0.913	0.857
IPO-LDM (RGB-D)	21.55	26.95	0.867	0.708	21.41	27.80	0.790	0.669	23.06	22.39	1.000	0.737	16.13	20.39	1.000	0.883

(a) **Mask types.** The proposed IPO-LDM is not sensitive to different mask types, and it outperforms the state-of-the-art models on all mask types.

Methods	Input Depth	FID ↓	sFID ↓	Density ↑	Coverage ↑
BIPS	fully visible	29.74	30.59	0.931	0.721
IPO-LDM (RGB-D)		21.90	26.78	0.829	0.693
BIPS	partial visible	31.70	28.89	0.769	0.660
IPO-LDM (RGB-D)		22.34	26.74	0.856	0.686
BIPS	fully masked	68.79	42.62	0.306	0.412
IPO-LDM (RGB-D)		21.55	26.95	0.867	0.708

(b) **Depth maps.** BIPS heavily relies on the availability of input depth, while our model is minimally affected. Notice that IPO-LDM with fully-masked depth even outperformed BIPS with fully-visible depth on s/FID.

Mask Type	SR	FID ↓	sFID ↓	Density ↑	Coverage ↑
Camera	-	24.29	28.05	0.805	0.663
	+	21.55	26.95	0.867	0.708
NFoV	-	23.96	28.19	0.775	0.645
	+	21.41	27.80	0.790	0.669

(c) **RefineNet.** (-): classical interpolation. (+): super-resolution. As expected, learning-based super-resolution leads to better results.

Table 2. **IPO-LDM ablations.** All models are trained and evaluated on the Structured3D dataset.

also considered the depth-conditioned LDM, mentioned in Section 3.3. However, it always produced blurry results (Fig. 8), so we leave out its quantitative results.

As can be seen, BIPS’s performance appears to deteriorate significantly when the input depth visual area is reduced. Conversely, our IPO-LDM is not sensitive to these depth maps, indicating that the generic model has successfully handled the modality. Interestingly, we noticed that having fully visible depth at test time did *not* improve the performance of our IPO-LDM, and in fact the result deteriorated slightly. A reasonable explanation for this situation is that during the training process, the signal-to-noise ratios (SNR) of RGB and depth pixels are roughly the same within each iteration, since no masks were used. However, during outpainting, the SNR balance will be disrupted when RGB input is masked and depth input is fully visible. Therefore, the results are degraded, but only slightly because IPO-LDM has effectively learnt the distribution of spatial visual patterns across all modalities, without being overly reliant on depth. This also explains why our model is more robust to depth inputs with different degrees of visibility.

Mask Types. As described in previous sections, our model is trained unconditionally, with masks only used during the inference phase. Therefore, our model is supposed to *be able to handle a greater range of mask types*, with performance less affected by the specific mask shape, and mainly by the area of the mask. To prove this, we tested and compared the performance of our model and the base-

line models under four different mask types, as described previously. As the performance of BIPS varies considerably depending on whether depth is visible or not, we listed both its performance when depth is partially visible (with depth), and when it is not visible at all (w/o depth).

The results are shown in Table 2a, which shows that both RGB and RGB-D IPO-LDM significantly outperform the baseline models for all types of masks, while RGB-D IPO-LDM achieved the best results. This indicates that LDM is able to perform outpainting of panoramas best, and also proves that the introduction of depth information significantly improves the quality of the generated RGB panorama.

Conversely, the performance of baseline models can vary considerably between mask types. For BIPS, although the difficulty between outpainting with camera masks and NFoV masks is not significant, the performance on camera masks is significantly better. This is likely due to BIPS using camera masks in the training process. In contrast, IPO-LDM has a more robust performance, producing high-quality and diverse output images for all mask distributions.

Two-end Alignment. Currently, there is no corresponding quantitative metric to evaluate the performance of aligning the two ends of an image. To make a more reasonable comparison, we make one side of the input image be fully visible, and the other side fully masked. Then compare the output with/without our rotational outpainting using the same model. To compare as many results, we only show the



Figure 9. **Examples of stitched ends of the outpainted images.** For each image, the left half was unmasked (*i.e.* ground truth), while the right half was masked and synthesized. Significant differences can be seen without the alignment mechanism (b) and in the results generated by OmniDreamer (c) and BIPS (d). In contrast, the results generated with rotation are more naturally connected at both ends (a).

end regions that are stitched together to highlight the contrast. The same tests were also performed on BIPS [25] and OmniDreamer [2].

The comparison results are shown in Fig. 9. They show that the consistency of the two ends of the results is improved after the use of rotational outpainting, especially the texture of the walls and the alignment of the layout. Still, differences can be found with rotated outpainting. We believe it is mainly due to the fact that rotational denoising is based on the latent level, which may introduce extra errors during decoding.

RefineNet. As described in Section 3.4, we trained a super-resolution model to increase the resolution of the input from 256×512 to 512×1024 as the second stage of our framework. Quantitative results on camera and N FoV masks are shown in Table 2c. The results show an overall increase in performance.

5. Discussion

Experimental results show that our model significantly outperforms baseline models on the 360° indoor RGB panorama outpainting task. Nevertheless, we consider several aspects of the model that can be further improved.

Depth Outpainting. We believe that IPO-LDM not only performs well for RGB outpainting but can also be used for depth image outpainting. The architecture we designed should in theory also be able to naturally synthesize RGB-D panoramas. In our experiments, however, depth generation did not perform well and contained non-negligible noise. From our analysis, we believe the reason for this issue is that the VQ model for depth modeling is not robust enough. Since the depth datasets used to train the LDM and VQ models are the same, latent depth can provide accurate information to assist RGB generation during training. However, during inference, the VQ model may not be able to accurately compress test depth input into the latent space. This may also explain why our model is inferior to BIPS in terms of coverage and density under the fully visible depth condition, as the depth information is not fully exploited. We hope that this problem can be solved in our subsequent work, which will lead to the simultaneous generation of consistent RGB-D panoramas.

Manipulable Panorama Outpainting. Even though our model is capable of generating diverse plausible results, it will be more meaningful to have a manipulable generative process. We will investigate such capabilities in the future. By using some simple prompts as conditions, the user can manipulate the generation of results, which enhances the usability of the model.

6. Conclusion

In this paper, we show that our proposed method, the two-stage RGB-D IPO-LDM, achieves state-of-the-art performance for indoor RGB panorama outpainting. The introduction of depth information via our bi-modal LDM structure significantly improves the performance of the model. Such improvement illustrates the effectiveness of using depth during training as an aid to guide RGB panorama generation. In addition, we show that the alignment mechanism we employ at each step of the denoising process of the diffusion model enhances the wraparound consistency of the results. With the use of these novel mechanisms, our two-stage structure is capable of generating high-quality RGB panoramas at 512×1024 resolution.

References

- [1] Naofumi Akimoto, Seito Kasai, Masaki Hayashi, and Yoshimitsu Aoki. 360-degree image completion by two-

- stage conditional gans. In *2019 IEEE International Conference on Image Processing (ICIP)*, pages 4704–4708. IEEE, 2019. 1, 3
- [2] Naofumi Akimoto, Yuhi Matsuo, and Yoshimitsu Aoki. Diverse plausible 360-degree image outpainting for efficient 3dcg background creation. In *Proceedings of the IEEE/CVF Conference on Computer Vision and Pattern Recognition*, pages 11441–11450, 2022. 1, 3, 6, 8
- [3] Andrew Brock, Jeff Donahue, and Karen Simonyan. Large scale gan training for high fidelity natural image synthesis. *arXiv preprint arXiv:1809.11096*, 2018. 2
- [4] Sungjoon Choi, Qian-Yi Zhou, and Vladlen Koltun. Robust reconstruction of indoor scenes. In *Proceedings of the IEEE Conference on Computer Vision and Pattern Recognition*, pages 5556–5565, 2015. 1
- [5] Alexei A Efros and Thomas K Leung. Texture synthesis by non-parametric sampling. In *Proceedings of the seventh IEEE international conference on computer vision*, volume 2, pages 1033–1038. IEEE, 1999. 2
- [6] Dave Epstein, Taesung Park, Richard Zhang, Eli Shechtman, and Alexei A Efros. Blobgan: Spatially disentangled scene representations. In *Computer Vision–ECCV 2022: 17th European Conference, Tel Aviv, Israel, October 23–27, 2022, Proceedings, Part XV*, pages 616–635. Springer, 2022. 1
- [7] Patrick Esser, Robin Rombach, and Bjorn Ommer. Taming transformers for high-resolution image synthesis. In *Proceedings of the IEEE/CVF conference on computer vision and pattern recognition*, pages 12873–12883, 2021. 3
- [8] Marc-André Gardner, Yannick Hold-Geoffroy, Kalyan Sunkavalli, Christian Gagné, and Jean-François Lalonde. Deep parametric indoor lighting estimation. In *Proceedings of the IEEE/CVF International Conference on Computer Vision*, pages 7175–7183, 2019. 1
- [9] Marc-André Gardner, Kalyan Sunkavalli, Ersin Yumer, Xiaohui Shen, Emiliano Gambaretto, Christian Gagné, and Jean-François Lalonde. Learning to predict indoor illumination from a single image. *ACM Transactions on Graphics (TOG)*, 36(6):1–14, 2017. 1
- [10] Ian Goodfellow, Jean Pouget-Abadie, Mehdi Mirza, Bing Xu, David Warde-Farley, Sherjil Ozair, Aaron Courville, and Yoshua Bengio. Generative adversarial networks. *Communications of the ACM*, 63(11):139–144, 2020. 1, 2
- [11] Takayuki Hara, Yusuke Mukuta, and Tatsuya Harada. Spherical image generation from a single image by considering scene symmetry. In *Proceedings of the AAAI Conference on Artificial Intelligence*, volume 35, pages 1513–1521, 2021. 3
- [12] Kaiming He and Jian Sun. Image completion approaches using the statistics of similar patches. *IEEE transactions on pattern analysis and machine intelligence*, 36(12):2423–2435, 2014. 2
- [13] Martin Heusel, Hubert Ramsauer, Thomas Unterthiner, Bernhard Nessler, and Sepp Hochreiter. Gans trained by a two time-scale update rule converge to a local nash equilibrium. *Advances in neural information processing systems*, 30, 2017. 5
- [14] Jonathan Ho, Ajay Jain, and Pieter Abbeel. Denoising diffusion probabilistic models. *Advances in Neural Information Processing Systems*, 33:6840–6851, 2020. 2
- [15] Daichi Horita, Jiaolong Yang, Dong Chen, Yuki Koyama, and Kiyoharu Aizawa. A structure-guided diffusion model for large-hole diverse image completion. *arXiv preprint arXiv:2211.10437*, 2022. 4
- [16] Zheng Hui, Jie Li, Xiumei Wang, and Xinbo Gao. Image fine-grained inpainting. *arXiv preprint arXiv:2002.02609*, 2020. 2
- [17] Satoshi Iizuka, Edgar Simo-Serra, and Hiroshi Ishikawa. Globally and locally consistent image completion. *ACM Transactions on Graphics (ToG)*, 36(4):1–14, 2017. 2
- [18] Jeong-Kyun Lee, Jaewon Yea, Min-Gyu Park, and Kuk-Jin Yoon. Joint layout estimation and global multi-view registration for indoor reconstruction. In *Proceedings of the IEEE international conference on computer vision*, pages 162–171, 2017. 1
- [19] Wenbo Li, Xin Yu, Kun Zhou, Yibing Song, Zhe Lin, and Jiaya Jia. Sdm: Spatial diffusion model for large hole image inpainting. *arXiv preprint arXiv:2212.02963*, 2022. 2
- [20] Hongyu Liu, Bin Jiang, Yibing Song, Wei Huang, and Chao Yang. Rethinking image inpainting via a mutual encoder-decoder with feature equalizations. In *Computer Vision–ECCV 2020: 16th European Conference, Glasgow, UK, August 23–28, 2020, Proceedings, Part II 16*, pages 725–741. Springer, 2020. 2
- [21] Andreas Lugmayr, Martin Danelljan, Andres Romero, Fisher Yu, Radu Timofte, and Luc Van Gool. Repaint: Inpainting using denoising diffusion probabilistic models. In *Proceedings of the IEEE/CVF Conference on Computer Vision and Pattern Recognition*, pages 11461–11471, 2022. 2, 4
- [22] Muhammad Ferjad Naeem, Seong Joon Oh, Youngjung Uh, Yunjey Choi, and Jaejun Yoo. Reliable fidelity and diversity metrics for generative models. In *International Conference on Machine Learning*, pages 7176–7185. PMLR, 2020. 5
- [23] Charlie Nash, Jacob Menick, Sander Dieleman, and Peter W Battaglia. Generating images with sparse representations. *arXiv preprint arXiv:2103.03841*, 2021. 5
- [24] Richard A Newcombe, Shahram Izadi, Otmar Hilliges, David Molyneaux, David Kim, Andrew J Davison, Pushmeet Kohi, Jamie Shotton, Steve Hodges, and Andrew Fitzgibbon. Kinectfusion: Real-time dense surface mapping and tracking. In *2011 10th IEEE international symposium on mixed and augmented reality*, pages 127–136. Ieee, 2011. 1
- [25] Changgyoon Oh, Wonjune Cho, Yujeong Chae, Daehee Park, Lin Wang, and Kuk-Jin Yoon. Bips: Bi-modal indoor panorama synthesis via residual depth-aided adversarial learning. In *Computer Vision–ECCV 2022: 17th European Conference, Tel Aviv, Israel, October 23–27, 2022, Proceedings, Part XVI*, pages 352–371. Springer, 2022. 1, 2, 3, 6, 8
- [26] Deepak Pathak, Philipp Krahenbuhl, Jeff Donahue, Trevor Darrell, and Alexei A Efros. Context encoders: Feature learning by inpainting. In *Proceedings of the IEEE conference on computer vision and pattern recognition*, pages 2536–2544, 2016. 2
- [27] Aditya Ramesh, Mikhail Pavlov, Gabriel Goh, Scott Gray, Chelsea Voss, Alec Radford, Mark Chen, and Ilya Sutskever. Zero-shot text-to-image generation. In *International Confer-*

- ence on Machine Learning, pages 8821–8831. PMLR, 2021. 3
- [28] Xiaofeng Ren, Liefeng Bo, and Dieter Fox. Rgb-(d) scene labeling: Features and algorithms. In *2012 IEEE Conference on Computer Vision and Pattern Recognition*, pages 2759–2766. IEEE, 2012. 2
- [29] Robin Rombach, Andreas Blattmann, Dominik Lorenz, Patrick Esser, and Björn Ommer. High-resolution image synthesis with latent diffusion models. In *Proceedings of the IEEE/CVF Conference on Computer Vision and Pattern Recognition*, pages 10684–10695, 2022. 1, 3, 5
- [30] Tim Salimans, Ian Goodfellow, Wojciech Zaremba, Vicki Cheung, Alec Radford, and Xi Chen. Improved techniques for training gans. *Advances in neural information processing systems*, 29, 2016. 1
- [31] Gowri Somanath and Daniel Kurz. Hdr environment map estimation for real-time augmented reality. In *Proceedings of the IEEE/CVF Conference on Computer Vision and Pattern Recognition*, pages 11298–11306, 2021. 1, 3
- [32] Shuran Song and Thomas Funkhouser. Neural illumination: Lighting prediction for indoor environments. In *Proceedings of the IEEE/CVF Conference on Computer Vision and Pattern Recognition*, pages 6918–6926, 2019. 1
- [33] Roman Suvorov, Elizaveta Logacheva, Anton Mashikhin, Anastasia Remizova, Arsenii Ashukha, Aleksei Silvestrov, Naejin Kong, Harshith Goka, Kiwoong Park, and Victor Lempitsky. Resolution-robust large mask inpainting with fourier convolutions. In *Proceedings of the IEEE/CVF winter conference on applications of computer vision*, pages 2149–2159, 2022. 6
- [34] Aaron Van Den Oord, Oriol Vinyals, et al. Neural discrete representation learning. *Advances in neural information processing systems*, 30, 2017. 3
- [35] Chuanxia Zheng, Tat-Jen Cham, and Jianfei Cai. Pluralistic image completion. In *Proceedings of the IEEE/CVF Conference on Computer Vision and Pattern Recognition*, pages 1438–1447, 2019. 2
- [36] Chuanxia Zheng, Tat-Jen Cham, Jianfei Cai, and Dinh Phung. Bridging global context interactions for high-fidelity image completion. In *Proceedings of the IEEE/CVF Conference on Computer Vision and Pattern Recognition*, pages 11512–11522, 2022. 6
- [37] Jia Zheng, Junfei Zhang, Jing Li, Rui Tang, Shenghua Gao, and Zihan Zhou. Structured3d: A large photo-realistic dataset for structured 3d modeling. In *Computer Vision—ECCV 2020: 16th European Conference, Glasgow, UK, August 23–28, 2020, Proceedings, Part IX 16*, pages 519–535. Springer, 2020. 2, 5